Traveling convection vortices induced by solar wind tangential discontinuities

R. Kataoka,[1] H. Fukunishi,[1] L. J. Lanzerotti,[2] T. J. Rosenberg,[3] A. T. Weatherwax,[3] M. J. Engebretson,[4] and J. Watermann[5]

Received 25 April 2002; revised 25 July 2002; accepted 20 August 2002; published 19 December 2002.

[1] Two typical magnetic impulse events (MIEs) accompanied by traveling convection vortices (TCVs) are investigated. The analysis of their conjugate equivalent convection patterns is performed using magnetic field data obtained from high-latitude ground magnetometer networks in the Northern and Southern Hemispheres. A three-dimensional analysis of solar wind structures is also performed using solar wind data obtained from multiple International Solar-Terrestrial Physics satellites. In the first event observed at ~1310 UT on 22 May 1996, a westward moving TCV appeared simultaneously in the noon-to-dawn sector in the Northern and Southern Hemispheres. The solar wind source of this TCV is found to be a tangential discontinuity (TD), which causes a rapid northward turning of the interplanetary magnetic field (IMF) and abrupt dynamic pressure changes. In the second event observed at ~1610 UT on 27 May 1998, an eastward moving TCV appeared in the noon sector in the Northern and Southern Hemispheres, with a timing delay of 2 to 3 min in the Southern Hemisphere. The solar wind source of this TCV is found again to be a TD, which causes a rapid IMF *By* negative turning and an abrupt enhancement of dynamic pressure. Analyses show that the TDs driving these events have their motional electric fields pointing toward the TDs and their normal vectors with large cone angles from the sunward direction. These TDs satisfy the conditions for the formation of a hot flow anomaly (HFA) at the bow shock. The sweeping motion across the magnetosphere of the intersection of the TD and the bow shock is found to be consistent with the observed TCV motion in each event. Magnetopause deformations due to HFAs can explain all the observed morphological features and the triggering process of these two MIEs. It is suggested, however, that bursty merging and/or pressure pulses would reinforce the processes produced by the HFAs, since the TDs are usually accompanied by both abrupt IMF changes and pressure enhancements. Consequently, it seems reasonable to conclude that the integrated processes of HFA, bursty magnetic field merging, and pressure pulses produce the evolution of these MIEs and TCVs. *INDEX TERMS:* 2784 Magnetospheric Physics: Solar wind/magnetosphere interactions; 2724 Magnetospheric Physics: Magnetopause, cusp, and boundary layers; 2708 Magnetospheric Physics: Current systems (2409); 2463 Ionosphere: Plasma convection; *KEYWORDS:* traveling convection vortex, magnetic impulse event, interplanetary tangential discontinuity

Citation: Kataoka, R., H. Fukunishi, L. J. Lanzerotti, T. J. Rosenberg, A. T. Weatherwax, M. J. Engebretson, and J. Watermann, Traveling convection vortices induced by solar wind tangential discontinuities, *J. Geophys. Res.*, *107*(A12), 1455, doi:10.1029/2002JA009459, 2002.

1. Introduction

[2] Magnetic impulse events (MIEs), with amplitudes ranging from several tens to several hundreds of nanoteslas and durations ranging from 5 to 20 min, are often observed in dayside high-latitude ground magnetograms [e.g., *Lanzerotti et al.*, 1991]. Because of their solitary features these MIEs are recognized as important entities for the investigation of transient magnetospheric responses to the passage of variable solar wind structures. It has been shown that many MIEs can be interpreted in terms of ionospheric Hall current loops associated with traveling convection vortices (TCVs) pass over the ground magnetometers

[1]Department of Geophysics, Tohoku University, Sendai, Japan.
[2]Bell Laboratories, Lucent Technologies, Murray Hill, New Jersey, USA.
[3]Institute for Physical Science and Technology, University of Maryland, College Park, Maryland, USA.
[4]Department of Physics, Augsburg College, Minneapolis, Minnesota, USA.
[5]Solar-Terrestrial Physics Division, Danish Meteorological Institute, Lyngbyvej, Copenhagen, Denmark.

0148-0227/02/2002JA009459

[e.g., *Friis-Christensen et al.*, 1988; *Glassmeier and Heppner*, 1992].

[3] Although various mechanisms including solar wind dynamic pressure pulses, bursty reconnection, plasma penetration, and the Kelvin-Helmholtz instability have been proposed, there is still no consensus on the sources and the generation mechanisms of TCVs and MIEs [*Kataoka et al.*, 2001, and references therein]. It has recently been suggested that hot flow anomalies (HFAs) formed at the bow shock are one of the important sources of MIEs. The comprehensive studies reported by *Sitar et al.* [1998] and *Sibeck et al.* [1999] provided evidence linking the orientation changes of the interplanetary magnetic field (IMF) to the occurrences of MIEs and TCVs. They suggested that HFAs produced by the interaction between solar wind tangential discontinuities (TDs) and the bow shock deform the magnetopause, driving tailward moving field-aligned currents and producing MIEs and/or TCVs.

[4] The purpose of this paper is to investigate solar wind discontinuities as a possible source of MIE/TCV events. We have studied two typical MIE/TCV events. We derive the equivalent ionospheric convection patterns from the analysis of conjugate ground magnetometer network data in the Northern and the Southern Hemispheres in order to understand the evolution of the three-dimensional (3-D) current systems producing MIE/TCV events. We then carry out a 3-D analysis of the solar wind data obtained from multiple International Solar-Terrestrial Physics (ISTP) satellites in order to illustrate the characteristics of the solar wind discontinuities.

2. Observations

[5] We selected two typical MIEs accompanied by TCVs observed on 22 May 1996 and 27 May 1998. These MIEs were selected by the same algorithm of *Lanzerotti et al.* [1991], using the three-component magnetometer data from South Pole (SP) station in Antarctica. One reason for the selection of these two events is that enough data from conjugate magnetometer network observations are available to derive equivalent convection patterns in the Northern and Southern Hemispheres. The second reason is that sufficient spacecraft data are available so that the 3-D features of the solar wind magnetic field and plasma can be determined for both events.

[6] We derive equivalent convection patterns in the Northern Hemisphere using magnetometer data from the Magnetometer Array for Cusp and Cleft Studies (MACCS) in Canada, the Canadian Auroral Network for the OPEN Program Unified Study (CANOPUS) sites, and Greenland coastal and ice cap stations. Equivalent convection patterns in the Southern Hemisphere are derived using magnetometer data from the Automatic Geophysical Observatories (AGOs), SP, and McMurdo (MM) in Antarctica, located near the magnetic conjugate regions of the MACCS and the Greenland magnetometers. IMF data and solar wind plasma data from the ACE, Wind, IMP 8, Geotail, and Interball satellites were used for study of the solar wind sources of these two events.

[7] In Figures 1 and 2, we illustrate the solar wind and ground signatures of these two MIEs on 22 May 1996 and 27 May 1998, respectively. The top seven and middle seven panels in Figures 1 and 2 show solar wind density, dynamic pressure, bulk speed, total IMF strength, and IMF B_x, B_y, and B_z variations in GSE coordinates, measured on both Wind and Geotail, respectively, for the 6-hour interval including the MIE timing. For both events, Wind was located more than 100 R_E upstream of the Earth's bow shock, while Geotail was located upstream but close to the bow shock (see below). The Geotail location is almost ideal to detect the direct features of solar wind impinging upon the dayside magnetosphere. In the bottom panel, geomagnetic vertical perturbations measured at a nearly conjugate pair of magnetometers, SP and Iqaluit (IQ) or SP and Pangnirtung (PG), are shown with bold and thin lines, respectively. The geographic and corrected geomagnetic (CGM) coordinates of these stations are summarized in Table 1. A comparison of the response timing and amplitudes observed at these north-south conjugate magnetometer stations provide important information for understanding the physical process of the connection between the dayside magnetosphere and the ionosphere. The timing represented by the vertical dotted line in the bottom panel of Figures 1 and 2 shows the onset of the MIE at SP, while the vertical dotted lines in the top and middle seven panels show the corresponding timing to the ground event at Wind and Geotail, respectively. The time lags between the satellites and ground are estimated considering the 3-D inclination of the solar wind discontinuity plane. The method used for the time lag estimation is described in the section 3.2.

[8] The MIE at ~1310 UT in the bottom panel in Figure 1 has a peak-to-peak amplitude of more than 100 nT in the vertical component at SP. The IQ magnetometer observed a similar impulsive feature with almost the same duration and amplitude. A positive vertical component pulse at 1312 UT, a negative pulse at 1315 UT, and a positive pulse at 1323 UT correspond to downward, upward, and downward field-aligned currents, respectively [see *Kataoka et al.*, 2001]. This interval is geomagnetically quiet with $Kp = 2$ and $\Sigma Kp = 10$ for the previous 24 hours.

[9] A rapid northward turning of the IMF B_z and a corresponding pressure enhancement with a density jump are found at the time corresponding to the onset of this MIE at both Wind at 1255 UT at GSE $(x, y, z) = (124.1, -24.2, -6.5)$ and Geotail at 1244 UT at GSE $(x, y, z) = (26.3, 10.6, -3.4)$. Note that the discontinuity occurred at the Geotail ~11 min before it was observed at Wind. This curious time delay can be explained by the 3-D inclination of the discontinuity

Figure 1. (opposite) Interplanetary data and ground-based geomagnetic field data for the interval 1000–1600 UT on 22 May 1996. Top and middle seven panels show the solar wind density (cm^{-3}), dynamic pressure (nPa), bulk speed (km/s), total interplanetary magnetic field (IMF) strength (nanoteslas), IMF B_x, B_y, and B_z component magnitudes (in nanoteslas and GSE coordinates) at Wind and Geotail, respectively. Bottom panel shows the vertical components of geomagnetic field data observed at South Pole (bold line) and Iqaluit (thin line) stations. Dotted vertical line shows the corresponding time at each position.

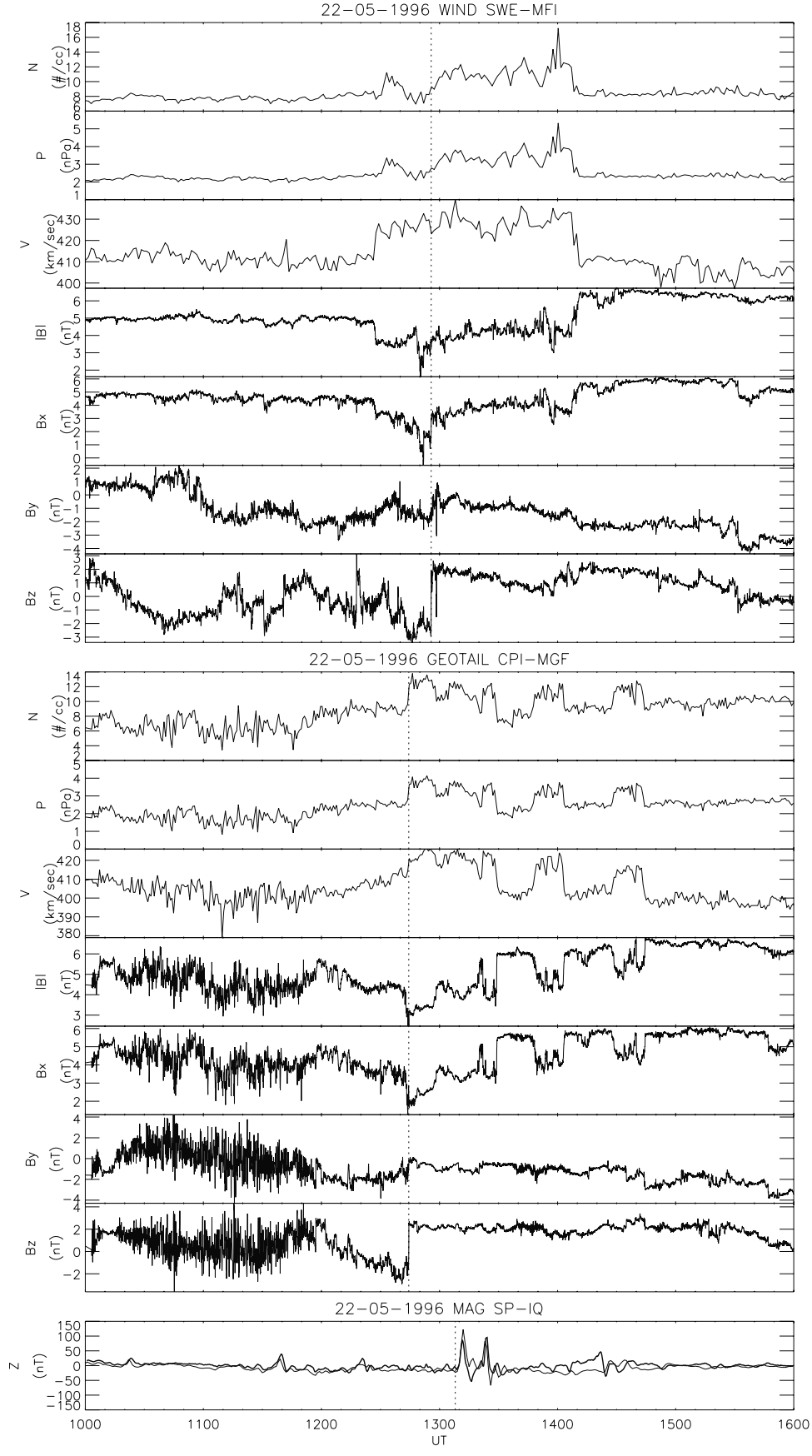
22−05−1996 WIND SWE−MFI
N (#/cc)
P (nPa)
V (km/sec)
|B| (nT)
Bx (nT)
By (nT)
Bz (nT)
22−05−1996 GEOTAIL CPI−MGF
N (#/cc)
P (nPa)
V (km/sec)
|B| (nT)
Bx (nT)
By (nT)
Bz (nT)
22−05−1996 MAG SP−IQ
Z (nT)
1000
1100
1200
1300
1400
1500
1600
UT

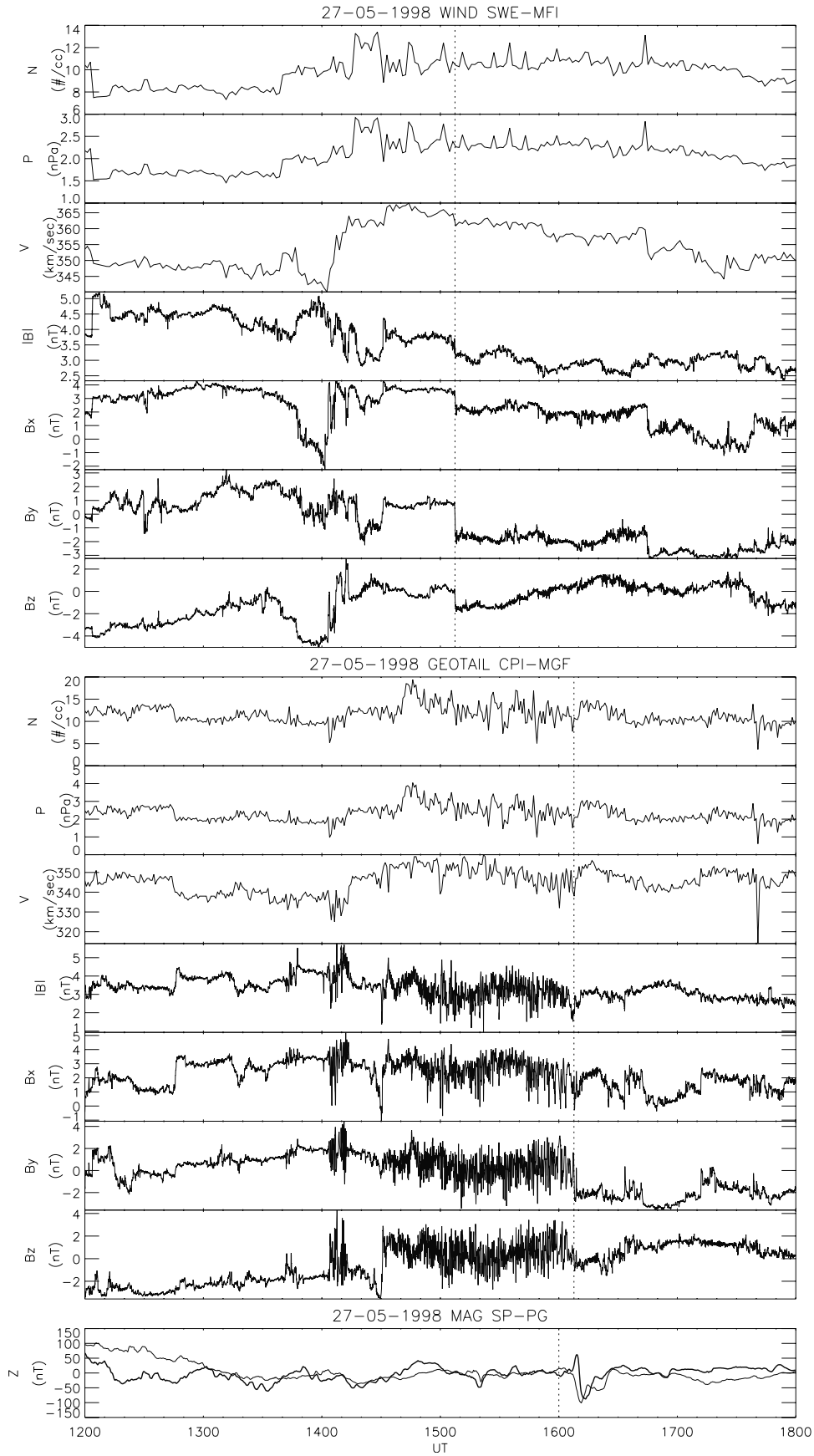

Figure 2. Interplanetary data and ground-based geomagnetic field data for the interval 1200–1800 UT on 27 May 1998. Format is the same as Figure 1.

Table 1. Geographic and Geomagnetic Coordinates of the Near Conjugate Magnetometer Stations

Station	GLAT	GLON	MLAT	MLON	UT-MLT
South Pole	−90.0	0.0	−74.0	18.9	0335
Iqaluit	63.8	291.5	73.1	15.0	0406
Pangnirtung	66.1	294.2	74.9	20.3	0346

plane, as is described in the section 3.2. The solar wind speed is almost stable at 420–440 km/s. Large-amplitude magnetic perturbations measured by Geotail during the interval 1000–1200 UT indicate that the spacecraft was within the foreshock. These perturbations reflect the widely spread ion foreshock due to the large IMF B_x component at that time.

[10] Figure 2 shows the MIE detected at ~1610 UT on 27 May 1998. The MIE has a peak-to-peak amplitude of more than 100 nT in the vertical component. The PG and SP magnetometer data show a similar impulsive feature with almost the same duration and amplitude. A time delay of 2 to 3 min is found between PG and SP, particularly in a negative pulse at ~1613 UT. A negative impulsive variation corresponds to an upward field-aligned current. This interval is also geomagnetically quiet with Kp = 1+ and ΣKp = 16 for the previous 24 hours.

[11] A rapid negative turning of the IMF By component is found at the time corresponding to the onset of this MIE at both Wind at GSE (x, y, z) = (192.4, 36.7, 25.7) and Geotail at GSE (x, y, z) = (21.5, 9.5, −2.9). The solar wind speed was almost steady at 340–360 km/s, while pressure variations with density jumps were ubiquitous at both Wind and Geotail for the interval 1400–1700 UT. Large-amplitude magnetic perturbations observed during the interval 1430–1610 UT show that Geotail was located within the foreshock for this time interval. This reflects again a widespread ion foreshock due to the large magnitude of the IMF B_x component at that time.

3. Results

3.1. Ionospheric Convection

[12] Equivalent ionospheric convection patterns in the Northern and Southern Hemispheres for the two events were derived by the method described by *Kataoka et al.* [2001]. The three-component magnetometer data from all of the arrays, CANOPUS, MACCS, Greenland chain, AGOs, SP, and MM, were used. Instantaneous two-dimensional (2-D) equivalent convection patterns, shown looking down on the dayside northern and southern ionosphere in CGM coordinates, are represented by arrows every 2 min in Figures 3 and 4. The lengths of the arrows are proportional to the convection velocities. Perturbations in the Z component are shown by superposed amplitude contours. Negative Z (shaded contour) signature designate the upward field-aligned current regions [see *Kataoka et al.*, 2001]. In the Northern Hemisphere, a clockwise convection vortex is consistent with a counterclockwise Hall current produced by an upward field-aligned current filament, while a counterclockwise convection vortex is consistent with a clockwise Hall current associated with a downward flowing field-aligned current. The rotation of the vortex is identically opposite in the Southern Hemisphere.

[13] The equivalent convection patterns in Figure 3 for the 22 May event show that at 1310 UT in the Northern Hemisphere, a two-cell convection pattern existed, with a counterclockwise vortex in the 0800–1200 MLT sector and a clockwise vortex in the 1200–1500 MLT sector. In addition, a strong poleward and duskward flow occurred around local magnetic noon at CGM latitudes (MLAT) 73°–80°. This flow changed its direction to equatorward and dawnward at 1316 UT, resulting in a reversed two-cell convection pattern in the 1000–1400 MLT sector at 1318 UT. The TCV guiding center moved westward at 70°–75° MLAT in the dawn-to-noon sector during the interval 1310–1318 UT. The speed of the TCV guiding center motion is 3–5 km/s at ionospheric altitude. The northern and southern convection patterns are almost identical. The amplitudes of the magnetic perturbations, however, are small in the Southern Hemisphere, except for comparable magnetic perturbations at SP and IQ.

[14] The equivalent convection pattern for the 27 May event (Figure 4) shows that at 1602 UT in the Northern Hemisphere, a counterclockwise vortex appears at ~1300 MLT and began to move toward the dusk. After the eastward passage of this vortex at 1608 UT, a clockwise convection vortex appeared around 1200 MLT and moved eastward and poleward at 72°–77° MLAT. The speed of the TCV center motion is 1 to 5 km/s at ionospheric altitude. The northern and southern convection flow patterns are almost identical, with a time delay of 2 to 3 min in the Southern Hemisphere. The amplitudes of the magnetic perturbations are small in the Southern Hemisphere, except for comparable magnetic perturbations at SP and IQ, which are both close to the center of the TCV.

[15] Seasonal effects on the magnetosphere and ionosphere may be the cause of some of the differences in the conjugate observations. Since these two events occurred approximately 1 month before summer solstice, the dipole equator is tilted significantly southward. The difference in the field line lengths from magnetospheric equatorial plane to the northern and to the southern ionosphere is large in this situation, especially in the magnetic noon sector. This transit time difference may be the cause of the time delay observed in the Southern Hemisphere in the 27 May 1998 event. The finding of no time delay in the 22 May 1996 event is consistent with the fact that the differences in the north-south field line lengths become smaller away from the magnetic noon sector. The smaller amplitudes of the overall magnetic perturbations in the Southern Hemisphere for both events are also consistent with the explanation that the total current input is smaller in the Southern Hemisphere than in the Northern Hemisphere due to lower conductivity in the austral winter season.

3.2. Solar Wind Discontinuity

[16] As described earlier, the characteristics of interplanetary conditions as related to the MIEs were obtained from solar wind data from ISTP satellites. It is necessary to know the normal vector **n** of a discontinuity plane in order to estimate the time lag T_{SP} from a satellite location **S** to a given location **P**,

$$T_{SP} = \frac{(\mathbf{P} - \mathbf{S}) \cdot \mathbf{n}}{\mathbf{V} \cdot \mathbf{n}}, \quad (1)$$

where **V** is the propagation velocity of the discontinuity. There are several ways to derive the normal vector of the

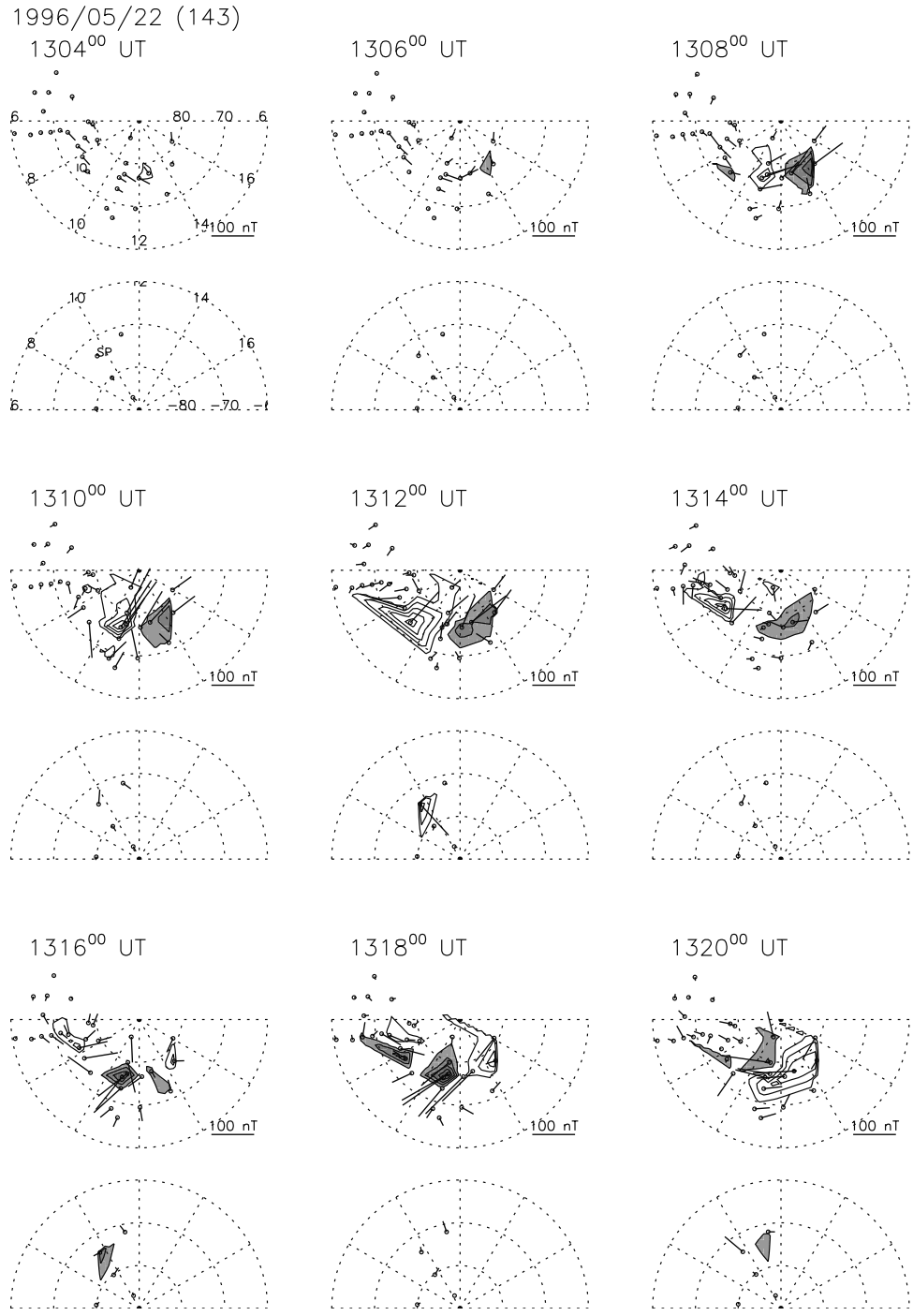

Figure 3. Equivalent convection patterns in the Northern and the Southern Hemispheres for the interval 1304–1320 UT on 22 May 1996. The contour lines and the shaded (white) areas show negative (positive) vertical amplitudes.

discontinuity plane. One of these methods uses multi-satellite data and derives a normal vector from the time lag of the discontinuity arrival at individual satellites, assuming a plane discontinuity and a constant propagation speed. In this study we used data from four satellites. The normal vector $\mathbf{n}_4$ is calculated as

$$\mathbf{n}_4 = \frac{(\mathbf{V}_{12} - \mathbf{V}_{13}) \times (\mathbf{V}_{12} - \mathbf{V}_{14})}{|(\mathbf{V}_{12} - \mathbf{V}_{13}) \times (\mathbf{V}_{12} - \mathbf{V}_{14})|}, \mathbf{V}_{ij} = \mathbf{R}_{ij}/T_{ij}, \quad (2)$$

where $\mathbf{R}_{ij}$ is the vector connecting satellite i and satellite j, and T_{ij} is the time lag from satellite i to satellite j. If the discontinuity is tangential, we can compute its normal simply as

$$\mathbf{n}_{\mathrm{TD}} = \frac{\mathbf{B}_1 \times \mathbf{B}_2}{|\mathbf{B}_1 \times \mathbf{B}_2|}, \quad (3)$$

where the subscripts 1 and 2 refer to the conditions prior to and after the arrival of a discontinuity, respectively. Note

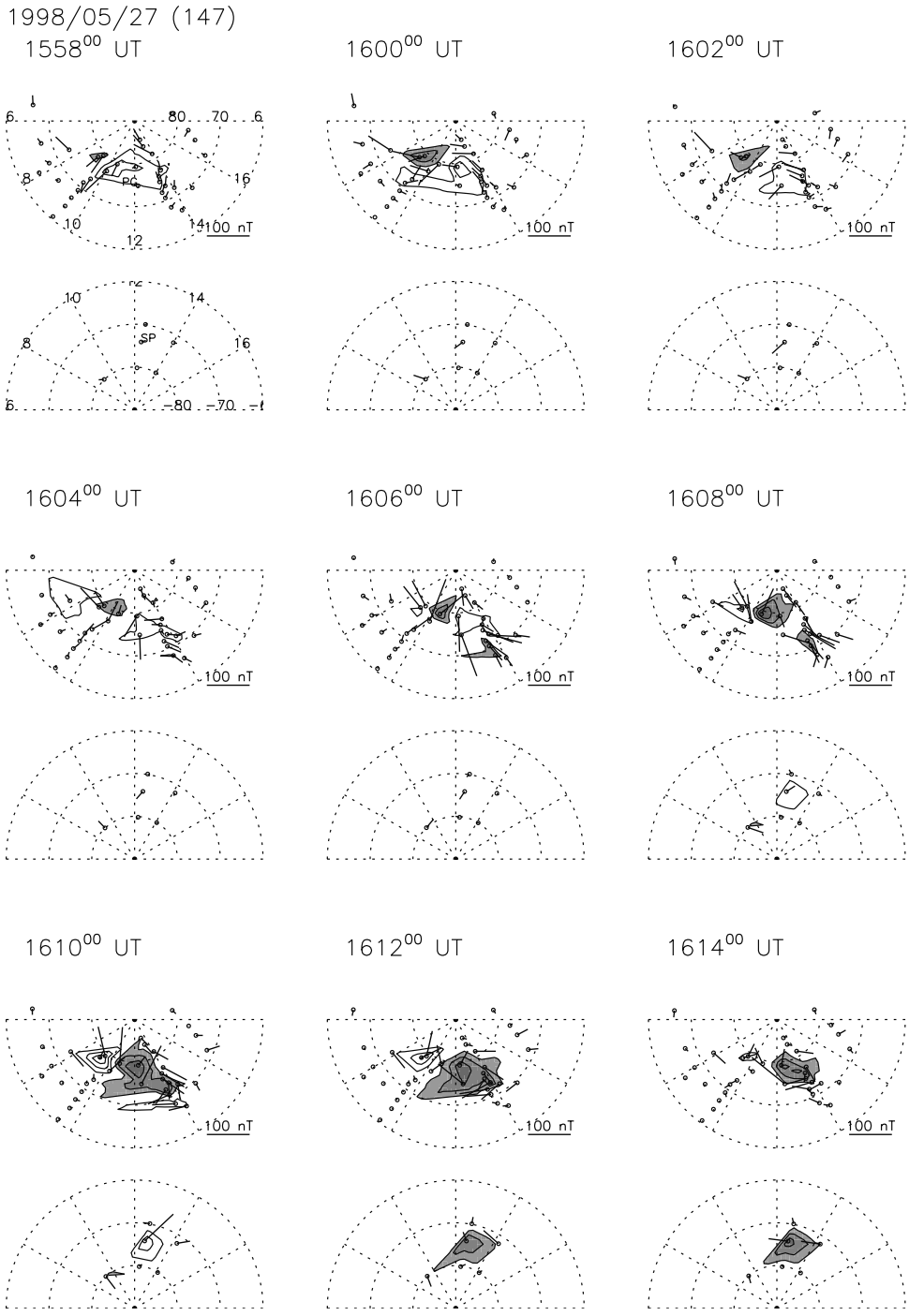

Figure 4. Equivalent convection patterns in the Northern and the Southern Hemispheres for the interval 1558–1614 UT on 27 May 1998. Format is the same as Figure 3.

that pre- and post-TD conditions are averaged ones for intervals of typically 1 to 2 min before and after the TD without including the TD itself. Another method estimates the normal vector from the minimum variance analysis (MVA) [*Sonnerup and Cahill*, 1967]. Since this method requires dozens of data points, we can use it when high time resolution (3-s) data are available.

[17] In the 22 May 1996 event all four satellites, Wind, IMP 8, Interball, and Geotail, observed similar discontinuities as a possible source of the MIE. The timing of IMF B_z northward turning is shown at each satellite location in Figure 5. For this event, $\mathbf{n}_4$ is calculated as GSE (x, y, z) = (-0.17, -0.85, 0.51). The three-component values of the $\mathbf{n}_{TD}$ vector at the four satellites are listed in Table 2, and their directions are depicted by arrows in Figure 5. All $\mathbf{n}_{TD}$ vectors are close to the $\mathbf{n}_4$ vector with only a small difference between the $\mathbf{n}_{TD}$ direction and the $\mathbf{n}_4$ direction (within $\sim 20^\circ$). It is also seen from the results in Table 2 that the $\mathbf{n}_{MVA}$ derived from the MVA method using Wind high time resolution (3-s) data is almost identical to $\mathbf{n}_{TD}$ at Wind. From these results, and considering the negligible value of $|\mathbf{B} \cdot \mathbf{n}|$ (~ 0.01 nT), we can conclude that this discontinuity is a TD.

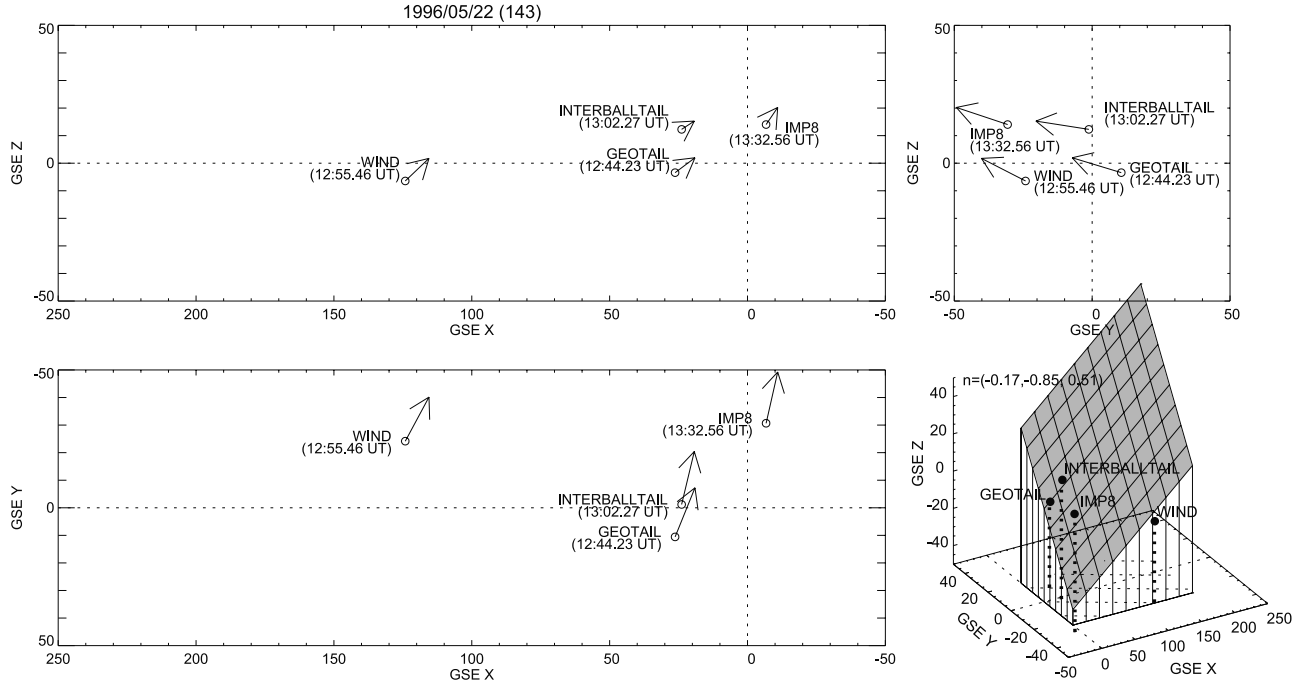

Figure 5. Locations, timing, and the normal vector of the tangential discontinuity observed at each satellite on 22 May 1996 showing (top left) GSE *X-Z* coordinates, (bottom left) GSE *X-Y* coordinates, and (top right) GSE *Y-Z* coordinates. (bottom right) Three-dimensional (3-D) view of the discontinuity plane used for timing calculation is also shown.

The feature of the inclined TD plane is displayed in a 3-D view in the right bottom panel of Figure 5.

[18] The solar wind conditions were more complicated in the 27 May 1998 event. Figure 6 shows the locations of available solar wind monitors, the passage timing of a sharp IMF B_y negative turning, and the normal vectors $\mathbf{n}_{TD}$ by arrows. Considering the results in Table 3, it is seen that the same IMF By negative turning was observed by Wind and Geotail (<20° difference in the direction of $\mathbf{n}_{TD}$), while ACE and IMP 8 observed somewhat different IMF By negative turnings (112° and 37° different from the normal derived from Wind, respectively). The time lag between Wind and Geotail was derived as ~65 min using the normal vector $\mathbf{n}_{TD}$ and the solar wind velocity **V** observed at Wind. Since the estimated lag is close to the actually observed value (~60 min), we consider that the discontinuities observed by both Wind and Geotail are identical. Almost identical three-component values of $\mathbf{n}_{TD}$ and $\mathbf{n}_{MVA}$ at Wind and a negligible value (~0.01 nT) of $|\mathbf{B} \cdot \mathbf{n}|$ imply that this discontinuity is also a TD. The right bottom panel of Figure 6 shows the 3-D geometry of the inclined TD plane. The solar wind discontinuity was almost parallel to the z = constant plane, and the locations of ACE and IMP 8 were largely offset from the solar ecliptic plane. Since the assumption of an infinite plane discontinuity is surely broken in such a situation, it is not unusual that ACE and IMP 8 did not observe the same discontinuity as that observed at Wind and Geotail.

[19] Figures 7a and 7b show the intersection of the TDs with the bow shock surface for the 22 May 1996 and the 27 May 1998 events, respectively. Dotted lines represent GSE X values of the bow shock surface. The bow shock model used here is from *Peredo et al.* [1995] for Alfvén Mach number M_A = 2 to 5, ignoring any IMF effects. The timing of the intersection is calculated using relation (1). In the timing calculation, $\mathbf{n}_4$ is used for the 22 May event, and $\mathbf{n}_{MVA}$ at Wind is used for the 27 May event. For simplicity, the solar wind velocity is fixed as (−420, 0, 0) km/s for the 22 May event, and (−360, 0, 0) km/s for the 27 May event. From Figure 7, we conclude that the timing is proper for the cause of each event, even taking into account the transition time from the bow shock to the magnetosphere and from the magnetosphere to the ionosphere. For each event, the signal transmission would take 6 to 7 min from the bow shock to the magnetopause, assuming that the propagation speed is Vsw/8 and the travel path in the magnetosheath is 3 *Re*. There would be an additional 1 to 2 min propagation from the magnetosphere to the ionosphere with an Alfvén speed of 1000 km/s and a magnetic field line length of 10–20 *Re*. These estimations are essentially based on the method of *Lockwood et al.* [1989] and references therein.

4. Discussion

[20] Important unresolved questions about MIE/TCV events include (1) what processes determine the location, motion, and north-south conjugacy of TCVs and (2) why

Table 2. Normal Vectors of a Discontinuity Observed on 22 May 1996

Satellite	Name	Timing, UT	Normal Vector in GSE
All	$\mathbf{n}_4$		(−0.17, −0.85, 0.51)
Wind	$\mathbf{n}_{TD}$	1255.46	(−0.43, −0.80, 0.41)
Wind	$\mathbf{n}_{MVA}$	1255.46	(−0.43, −0.85, 0.29)
Geotail	$\mathbf{n}_{TD}$	1244.23	(−0.36, −0.95, 0.13)
Interball	$\mathbf{n}_{TD}$	1302.27	(−0.23, −0.96, 0.15)
IMP 8	$\mathbf{n}_{TD}$	1332.56	(−0.21, −0.93, 0.31)

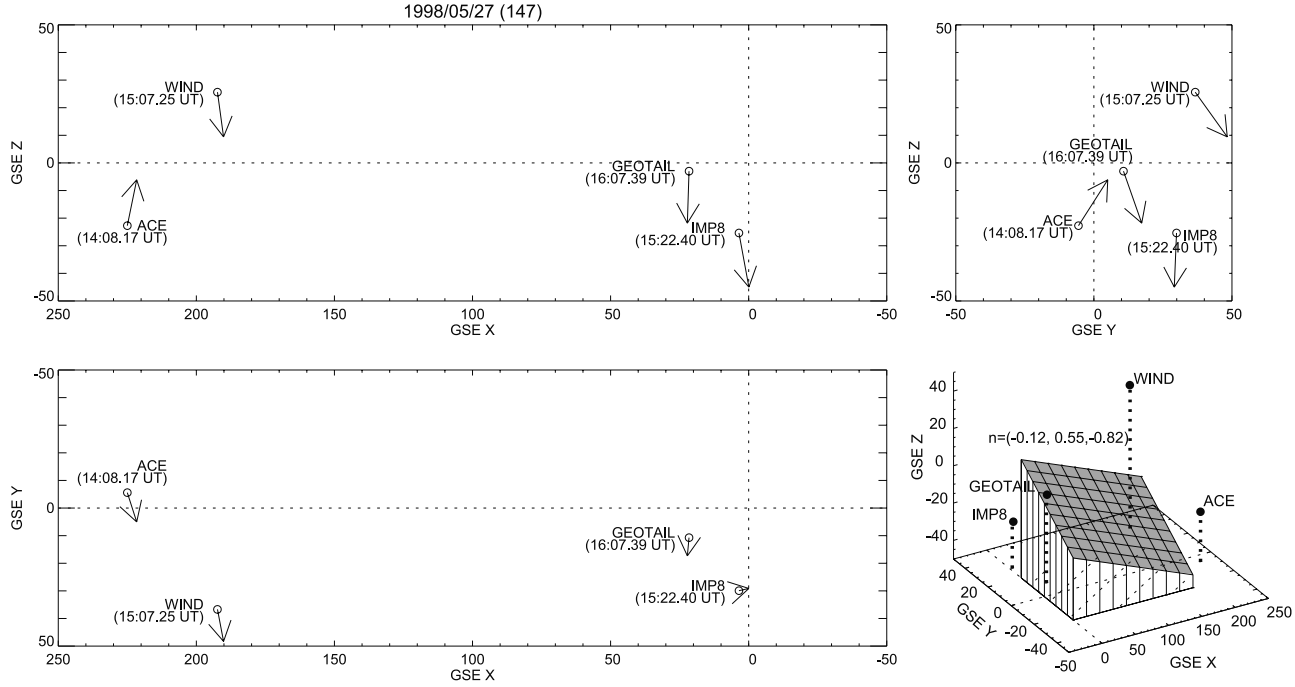

Figure 6. Locations, timing, and the normal vector of the tangential discontinuity observed at each satellite on 27 May 1998, showing (top left) GSE *X-Z* coordinates, (bottom left) GSE *X-Y* coordinates, and (top right) GSE *Y-Z* coordinates. (bottom right) Three-dimensional view of the discontinuity plane used for timing calculation is also shown.

only particular TDs seem to trigger MIEs. First, in order to investigate whether HFAs could be a possible source of MIEs/TCVs, we evaluated the necessary geometric relation between the TD and the bow shock.

[21] There are at least two criteria for producing HFA at the bow shock. The first criterion is the transit speed of the TD along the bow shock. The kinetic description of the creation of a HFA is that of reflected ions being channeled upstream along the current sheet. This description suggests one possible restriction: that the intersection of the current sheet with the bow shock must move sufficiently slowly along the bow shock to enable the reflected ions to remain close to and interact with the current sheet. The requirement of TDs whose normal vectors have large cone angles (>60°) with small normalized transit velocities (<0.3) has been suggested from the statistical analysis of HFAs by *Schwartz et al.* [2000].

[22] The second criterion is concerned with the motional electric field vector accompanying the TD. TDs create HFAs when the motional electric field is oriented toward the TD on one or both sides of it. The directional test proposed by *Thomsen et al.* [1993] was used in this paper. The condition of inward pointing motional electric field can be checked by the relationship of $\theta_1 > 90°$ and $\theta_2 < 90°$, where

$$\theta_j = \cos^{-1} \frac{\mathbf{n} \cdot (\mathbf{B}_j \times \mathbf{V}_{SW})}{\mathbf{B}_j \times \mathbf{V}_{SW}}. \quad (4)$$

[23] The TDs in both events have normal vectors with very large (>80°) cone angles as is shown by the arrows in Figures 5 and 6. The normalized transit velocity of the TD was <0.3 everywhere on the bow shock for at least one side of the TD for each event. The TDs also satisfy the condition of inward pointing motional electric field as $\theta_1 = 164°$ and $\theta_2 = 44°$ in the 22 May 1996 event and as $\theta_1 = 151°$ and $\theta_2 = 9°$ in the 27 May 1998 event. From these results, both TDs satisfy the conditions for the formation and evolution of HFA at the bow shock. Once a HFA is formed at the bow shock, the HFA structure should move with the intersection of the TD and the bow shock [*Sibeck et al.*, 2000]. TCVs caused by HFAs will move mainly in the longitudinal direction along the azimuthal sweep motion of the intersection line. The westward motion of the TCV on 22 May 1996 is consistent with the dawnward sweep motion of the intersection line, and the eastward motion of the TCV on 27 May 1998 is also consistent with the duskward sweep motion of the intersection line as shown in Figures 7a and 7b, respectively.

[24] Snapshots of the TCVs and the expected deformations of the dayside magnetosphere at 1310 and 1316 UT in the 22 May 1996 event and at 1604 UT in the 27 May 1998 event are schematically shown in Figures 8a and 8b, respectively. The formation of the HFA is assumed to start near the nose of the magnetosphere where the HFA is preferentially formed [*Schwartz et al.*, 2000]. The possible

Table 3. Normal Vectors of a Discontinuity Observed on 27 May 1998

Satellite	Name	Timing, UT	Normal Vector in GSE
Wind	$\mathbf{n}_{TD}$	1507.25	(−0.11, 0.58, −0.81)
Wind	$\mathbf{n}_{MVA}$	1507.25	(−0.12, 0.55, −0.82)
Geotail	$\mathbf{n}_{TD}$	1607.39	(0.03, 0.33, −0.94)
Ace	$\mathbf{n}_{TD}$	1408.17	(−0.17, 0.53, 0.83)
IMP 8	$\mathbf{n}_{TD}$	1522.40	(−0.18, −0.04, −0.98)

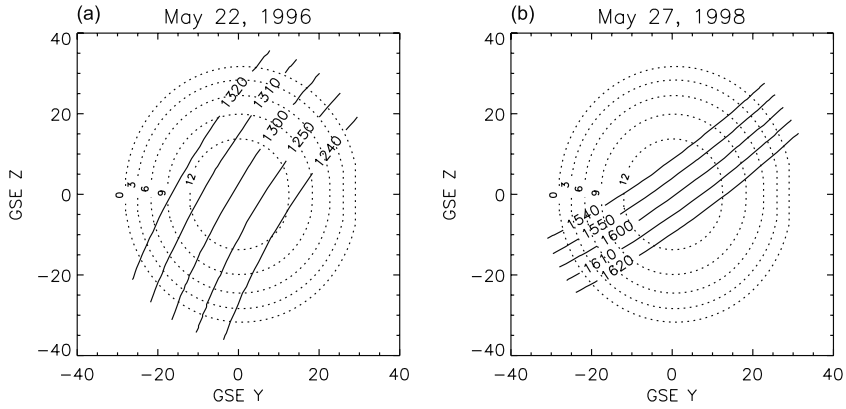

Figure 7. The intersection of the tangential discontinuities (solid lines) and the bow shock at 10-min intervals in GSE *Y-Z* coordinates for (a) 1240–1320 UT on 22 May 1996 and (b) 1540–1620 UT on 27 May 1998. Dotted lines show the GSE *X* component of the bow shock surface.

effects of pressure pulses and bursty flows due to antiparallel dayside reconnection are also schematically illustrated in Figure 8. Basically, HFAs and pressure pulses deform the magnetosphere outward and inward, respectively [*Sibeck et al.*, 2000]. The deformation of the magnetopause produces field-aligned currents via vortical plasma flows and/or divergence of the inertia currents in the closed boundary region (reviewed by *Cowley* [2000]). On the other hand, antiparallel reconnection would work as a voltage generator to produce field-aligned currents in both open and closed field line regions via merging of the solar wind motional electric field into the magnetosphere [*Glassmeier and Heppner*, 1992].

[25] It is worthwhile to note that the downward, upward, and downward field-aligned triplet structure at 1316 UT in Figure 8a is very similar to the TCVs due to HFA described

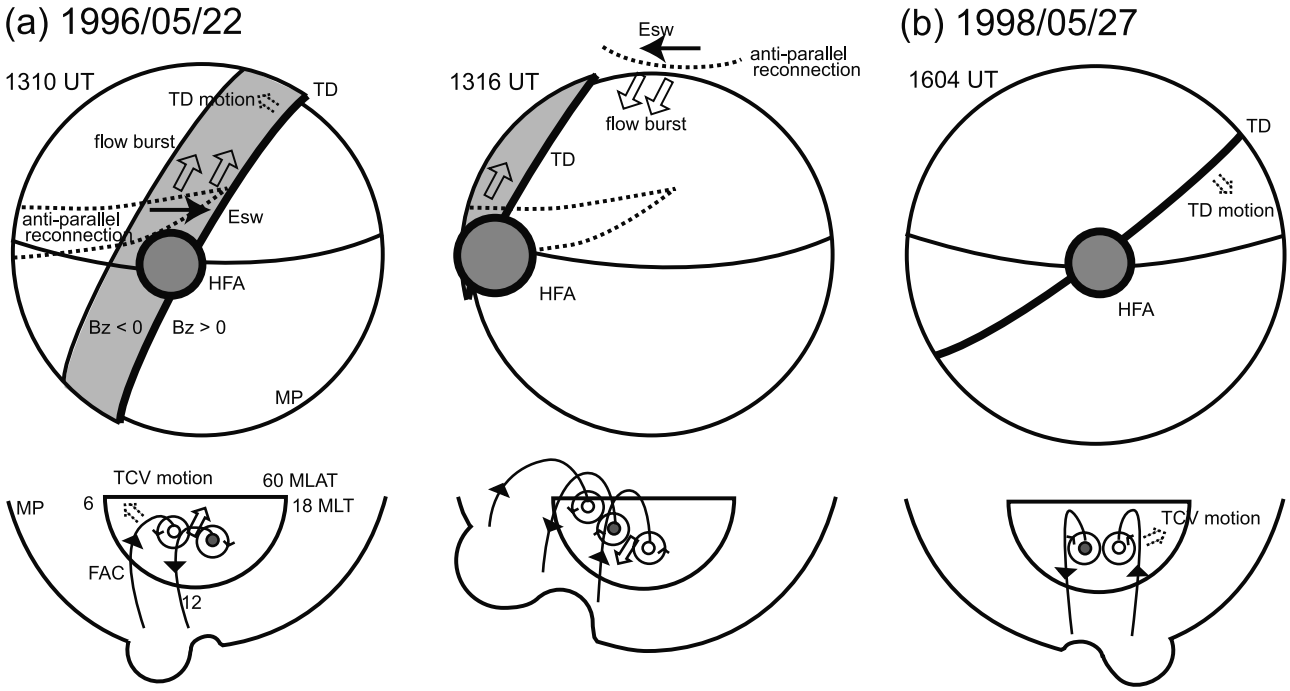

Figure 8. Summary sketches of the traveling convection vortices and expected deformations of the dayside magnetosphere associated with the tangential discontinuities at (a) 1310 and 1316 UT in the 22 May 1996 event and at (b) 1604 UT in the 27 May 1998 event. In the top panels, possible effects of pressure pulses and bursty flows due to antiparallel dayside reconnection are schematically illustrated with 3-D view of the dayside magnetopause. Dotted lines show the expected regions of antiparallel reconnection, and merging electric fields are denoted as Esw. In the bottom panels, equatorial cuts of the dayside magnetopause are depicted with field-aligned currents flowing into or out of the northern polar ionosphere. Shaded and open circles represent the guiding centers of clockwise and counterclockwise vortices, respectively.

by *Sitar et al.* [1998]. The first pair of leading downward and trailing upward field-aligned currents observed in the noon sector at 1310 UT in Figure 8a matches the two-cell convection pattern with a strong poleward flow around magnetic noon, and the second pair of leading upward and trailing downward field-aligned currents observed in the same sector at 1316 UT matches to reversed two-cell convection pattern with a strong equatorward flow around magnetic noon. The effects of the magnetopause deformation in the closed field line region could then be expected to produce the conjugate magnetic perturbations in the Northern and Southern Hemispheres. Similarly, the pair of leading downward and trailing upward field-aligned currents observed in the noon sector at 1604 UT in Figure 8b is also produced by the magnetopause deformation due to both the HFA cavity and the pressure enhancement at its edge. Antiparallel reconnection is not suggested for the 27 May 1998 event in Figure 8b because there is no clear IMF B_z jump at the TD arrival at Geotail. In summary, all of the morphological features of these two events can be explained by the HFA mechanism.

[26] We found several additional pieces of evidence that support the conclusion that only the HFA mechanism can select the appropriate solar wind discontinuities for the generation of MIEs, even though there are generally many IMF B_z turnings or pressure pulses in the solar wind. No MIEs were produced on the ground during the 22 May event interval by the pressure pulses that were measured at Geotail at 1345 UT and 1430 UT (see Figure 1) even though these had amplitudes and timescales similar to those of the TD that produced the MIE event (1244 UT). Similarly, in the interval of the 27 May 1998 event, the abrupt pressure enhancement observed at Geotail at 1607 UT is not unusual; pressure enhancements with comparable amplitudes and timescales are found at many times in the data interval (see Figure 2). These observations demonstrate that the pressure pulse model alone is not sufficient to explain the triggering process of MIEs.

[27] It is also worthwhile to note that an IMF B_z northward turning at Geotail at 1430 UT on 27 May 1998 (see Figure 2) is similar to the TD at Geotail at 1244 UT on 22 May 1996 (see Figure 1). A comparison between these two similar northward turnings indicates that the bursty merging model alone can not explain the triggering process of MIEs. The normal vector of the discontinuity at 1430 UT on 27 May 1998 is derived from relation (2) as $\mathbf{n}_4 = (-0.31, 0.95, -0.04)$. This normal vector $\mathbf{n}_4$ is close to the $\mathbf{n}_{TD}$ value observed at ACE, Wind, IMP 8, and Geotail, and its direction difference from $\mathbf{n}_{TD}$ is within 10°. From these results, and considering a negligible value of $|\mathbf{B} \cdot \mathbf{n}|$, we can conclude that this discontinuity is also a TD. This TD is characterized by a relatively strong southward IMF component (~ -4 nT) several minutes before the TD passage and a sharp northward IMF turning ($\sim$2 nT) and an abrupt pressure enhancement after the TD passage. Although these features are very similar to the TD that was measured at 1244 UT on 22 May 1996, ground magnetometers did not observe any MIE/TCV events at the estimated arrival time ($\sim$1430 UT), as shown in the bottom panel of Figure 2. This TD satisfies the first criterion for HFA formation: the normal vector has a large cone angle (>60°) with a small value of normalized transit velocity (<0.3). However, the second criterion is not satisfied; that is, the motional electric field is outward at both sides of the TD; that is, $\theta_1 = 19°$ and $\theta_2 = 124°$. Therefore we conclude that the reason why the TD at 1430 UT at Geotail on 27 May 1998 did not produce a MIE/TCV event is the absence of one of the criteria for HFA formation at the bow shock.

[28] As discussed above, although magnetopause deformations due to HFA formation can explain all the observed morphological features and the triggering process of these two MIEs/TCVs, it is essential to consider the effects of reconnection and pressure pulse effects, since interplanetary TDs often exhibit abrupt north-south IMF turnings and the enhancement of dynamic pressure simultaneously. It is worthwhile to note that a strong poleward and duskward flow around the magnetic noon meridian at 1310 UT in the 22 May 1996 event can also be interpreted as a result of bursty merging at the dayside magnetopause that is caused by a relatively strong southward and dawnward IMF observed several minutes before the TD passage. The average values of the IMF in this interval are approximately GSE $(x, y, z) = (2.0, -1.5, -2.0)$. Considering the topology of the antiparallel reconnection, both flow bursts and magnetic tension caused by the dayside reconnection should be directed poleward and duskward in the northern magnetopause (see Figure 8a).

[29] On the other hand, the reversed two-cell convection pattern with an equatorward flow around magnetic noon at 1316 UT may also be interpreted as a bursty flow due to high-latitude reconnection caused by a rapid northward IMF turning ($\sim$2 nT) after the TD passage. Since the change of the large-scale convection pattern propagates tailward on a similar time scale (4–13 min) and with a propagation velocity at $\sim$1.5 MLT/min [see *Murr and Hughes*, 2001], the transition of the large-scale convection pattern itself could become the traveling convection vortex.

[30] The dotted lines in Figure 8a show the expected regions of antiparallel reconnection inferred from the criterion of *Rodger et al.* [2000] under the IMF conditions of southward B_z and negative B_y in summer solstice. We might expect that the first pair of leading downward and trailing upward field-aligned currents derived from the northern magnetometer networks is associated with the eastward merging electric field (denoted as Esw in Figure 8a) because of dayside reconnection. Since the magnetopause counter current flows from dusk to dawn it gives rise to a system of downward field-aligned currents on the morning side and upward currents in the noon sector [see *Glassmeier and Heppner*, 1992, Figure 11]. Such field-aligned currents occur naturally because of considerations of current continuity. In a similar manner, we expect that the second pair of leading upward and trailing downward field-aligned currents is associated with the westward merging electric field at high latitude. The current system produced by this merging scenario does not conflict with the HFA current system. Furthermore, the current system produced by a pressure jump at the TD also does not conflict with the current system of the HFA mechanism. A HFA not only has a density-pressure decrease in the core but also a density-pressure pulse at the edge [*Sibeck et al.*, 1999, 2000]. The preexistent pressure enhancement at the TD would be further reinforced by the density-pressure pulse at the trailing edge of the HFA. Such a pair of localized rarefaction

and compression regions might produce a much stronger gradient in the magnetopause deformation and produce further impulsive current systems.

[31] Summarizing the above discussion, an integrated model including the effects of not only a HFA but also the effect of bursty merging and pressure pulses as schematically shown in Figure 8 is required. Given an integrated model, it would be possible to clarify the physical processes that select the source of MIE/TCV events from a series of pressure pulses or IMF B_z turnings in the solar wind. As the next step, a quantitative approach is needed to assess and confirm this concept. For example, why the TCV current system is transient and asymmetric in the Northern and Southern Hemispheres is one of the most interesting questions. The present wide spatial separation of the magnetometer stations, especially in the Southern Hemisphere, makes this a remaining open question. A simulation using a magnetosphere-ionosphere coupling model including a north-south asymmetry [e.g., *Nakata et al.*, 2000] is a good starting point to investigate this problem. Further, it is extremely important to carry out measurements of magnetic perturbations with much denser arrays (with $\sim$100 km separation) of magnetometers both in the northern and southern polar regions, combined with in situ spacecraft measurements in the vicinity of the magnetopause and the bow shock. The Cluster mission array may contribute to this latter experiment objective.

5. Conclusion

[32] We investigated two typical magnetic impulse events (MIEs) accompanied by traveling convection vortices (TCVs) in the Northern and the Southern Hemispheres from analyses of equivalent ionosphere convection patterns and solar wind discontinuities. New findings are as follows:

1. The solar wind sources of these MIE/TCV events are found to be interplanetary tangential discontinuities (TDs) exhibiting a rapid turning of the interplanetary magnetic field (IMF) and abrupt dynamic pressure changes.

2. These TDs satisfy the criteria for HFA formation at the bow shock. That is, the TDs have inward pointing motional electric fields at both sides of the TDs, and the normal vectors have large cone angles with respect to the sunward direction. The sweeping motions of the intersection lines of the TDs and the Earth's bow shock are also consistent with the observed TCV motions.

3. Although magnetopause deformations due to HFAs can explain all the observed morphological features and the triggering process of these MIE/TCV events, pressure pulses or bursty merging alone can not explain all of these features.

[33] It is suggested, however, that bursty merging and/or pressure pulses would reinforce the processes produced by HFAs, since the TDs are usually accompanied by both abrupt IMF changes and pressure enhancements. Consequently, it seems reasonable to conclude that the integrated processes of HFA, bursty merging, and pressure pulse produce the evolution of MIEs and TCVs.

[34] **Acknowledgments.** We express our sincere thanks to all members of the geomagnetic field observation network teams: the Greenland chain, the CANOPUS, and the MACCS, and the PENGUIn AGO array in Antarctica. Data from Greenland ice cap magnetometers (MAGIC) were kindly provided by C. R. Clauer, SPRL, University of Michigan, with support from the National Science Foundation. Also, thanks are extended to T. Hughes for magnetometer data from CANOPUS. The CANOPUS instrument array was constructed, maintained, and operated by the Canadian Space Agency for the Canadian scientific community. The MACCS array was supported by the Atmospheric Science Division of the U.S. National Science Foundation. Acquisition of Antarctic magnetometer data from South Pole, McMurdo, and AGOs was supported by the Office of Polar Programs, U.S. National Science Foundation. We acknowledge the ACE, Wind, IMP 8, Geotail, and Interball working teams for the magnetic field and plasma data. We also thank the very helpful system of the NASA NSSDC ISTP program (CDAWeb, SpyCAT, SSCWeb) and related PIs for allowing the browsing of useful key parameter data from many satellites consulted in the preparation of this paper.

[35] Lou-Chuang Lee and Chin S. Lin thank David G. Sibeck and C. Robert Clauer for their assistance in evaluating this paper.

References

Cowley, S. W., Magnetosphere-ionosphere interactions: A tutorial review, in *Magnetospheric Current Systems*, *Geophys. Monogr. Ser.*, vol. 118, edited by S. Ohtani et al., pp. 91–106, AGU, Washington, D. C., 2000.

Friis-Christensen, E., M. A. McHenry, C. R. Clauer, and S. Vennerstrom, Ionospheric traveling convection vortices observed near the polar cleft: A triggered response to sudden changes in the solar wind, *Geophys. Res. Lett.*, *15*, 253, 1988.

Glassmeier, K. H., and C. Heppner, Traveling convection twin vortices: Another case study, global characteristics, and a model, *J. Geophys. Res.*, *97*, 3977, 1992.

Kataoka, R., H. Fukunishi, L. J. Lanzerotti, C. G. Maclennan, H. U. Frey, S. B. Mende, J. H. Doolittle, T. J. Rosenberg, and A. T. Weatherwax, Magnetic impulse event: A detailed case study of extended ground and space observations, *J. Geophys. Res.*, *106*, 25,873, 2001.

Lanzerotti, L. J., R. M. Konik, and A. Wolfe, Cusp latitude magnetopause events, 1, Occurrence statistics, *J. Geophys. Res.*, *96*, 14,009, 1991.

Lockwood, M., P. E. Sandholt, S. W. H. Cowley, and T. Oguti, Interplanetary magnetic field control of dayside auroral activity and the transfer of momentum across the dayside magnetopause, *Planet. Space Sci.*, *37*, 1347, 1989.

Murr, D. L., and W. J. Hughes, Reconfiguration timescales of ionospheric convection, *Geophys. Res. Lett.*, *28*, 2145, 2001.

Nakata, H., S. Fujita, A. Yoshikawa, M. Itonaga, and K. Yumoto, Ground magnetic perturbations associated with the standing toroidal mode oscillations in the magnetosphere-ionosphere system, *Earth Planets Space*, *52*, 601, 2000.

Peredo, M., J. A. Slavin, E. Mazur, and S. A. Curtis, Three-dimensional position and shape of the bow shock and their variation with Alfvenic, sonic and magnetosonic Mach numbers and interplanetary magnetic field orientation, *J. Geophys. Res.*, *100*, 7907, 1995.

Rodger, A. S., I. J. Coleman, and M. Pinnock, Some comments on transient and steady-state reconnection at the dayside magnetopause, *Geophys. Res. Lett.*, *27*, 1359, 2000.

Schwartz, S. J., G. Paschman, N. Sckopke, T. M. Bauer, M. Dunlop, A. N. Fazakerley, and M. F. Thomsen, Conditions for the formation of hot flow anomalies at Earth's bow shock, *J. Geophys. Res.*, *105*, 12,639, 2000.

Sibeck, D. G., et al., Comprehensive study of the magnetospheric response to a hot flow anomaly, *J. Geophys. Res.*, *104*, 4577, 1999.

Sibeck, D. G., et al., Magnetopause motion driven by interplanetary magnetic field variations, *J. Geophys. Res.*, *105*, 25,155, 2000.

Sitar, R. J., J. B. Baker, C. R. Clauer, A. J. Ridley, J. A. Cumnock, V. O. Papitashvili, J. Spann, M. J. Brittnacher, and G. K. Parks, Multi-instrument analysis of the ionospheric signatures of a hot flow anomaly occurring on June 24, 1996, *J. Geophys. Res.*, *103*, 23,357, 1998.

Sonnerup, B. U. O., and L. J. Cahill Jr., Magnetopause structure and attitude from Explorer 12 observations, *J. Geophys. Res.*, *72*, 171, 1967.

Thomsen, M. F., V. A. Thomas, D. Winske, J. T. Gosling, M. H. Farris, and C. T. Russell, Observational test of hot flow anomaly formation by the interaction of a magnetic discontinuity with the bow shock, *J. Geophys. Res.*, *98*, 15,319, 1993.

M. J. Engebretson, Department of Physics, Augsburg College, Minneapolis, MN 55454, USA.

J. H. Fukunishi and R. Kataoka, Department of Geophysics, Tohoku University, Sendai, 980-8578, Japan.

L. J. Lanzerotti, Bell Laboratories, Lucent Technologies, Murray Hill, NJ 07974, USA.

T. J. Rosenberg and A. T. Weatherwax, Institute for Physical Science and Technology, University of Maryland, College Park, MD 20742, USA.

J. Watermann, Solar-Terrestrial Physics Division, Danish Meteorological Institute, Lyngbyvej, 100 DK-2100 Copenhagen, Denmark.